ELSEVIER

Polymer 41 (2000) 5367–5374

polymer

Micellization behavior of diblock copolymers in solution near the critical micelle temperature

Y. Fukumine[a], K. Inomata[a], A. Takano[b], T. Nose[a,*]

[a]*Department of Polymer Chemistry, Tokyo Institute of Technology, 2-12-1 Ookayama, Meguro-ku, Tokyo 152-8552, Japan*
[b]*Department of Applied Chemistry, Nagoya University, Furo-cho, Chigusa-ku, Nagoya 464-8603, Japan*

Received 16 July 1999; received in revised form 20 September 1999; accepted 24 September 1999

Abstract

Micellization behavior near the critical micelle temperature (c.m.t.) has been studied for polystyrene-*block*-poly(dimethylsiloxane) (PS-*b*-PDMS) in a mixed solvent of 1,2-dichlorobenzene/benzyl alcohol, which forms micelles with PDMS as cores. Static and dynamic light scattering experiments have demonstrated the following behaviors. The dilute solution ($c \cong 0.1$–4 wt%) shows three different characteristic behaviors depending on the copolymer concentration c. In the concentrated region, the temperature dependence of scattered-light intensity exhibits a large peak just below c.m.t., which is similar to the anomalous micellization. Detailed light scattering studies have revealed the following: in this concentration region, compact micelles are formed at low temperatures and as the temperature is increased, the micelles change into expanded swollen micelles discontinuously at a certain temperature. This change occurs rather reversibly, and may be explained by a strong condensation of the core due to the decrease in solvent quality with decreasing temperature. This can be a mechanism of the anomalous micellization.

Keywords: Diblock copolymer; Micelle; Anomalous micellization

1. Introduction

Diverse association behaviors of block copolymers in selective solvents have extensively been studied from both theoretical and experimental viewpoints [1]. In these studies it has been demonstrated that the block copolymer micellization is essentially a closed association, exhibiting the critical micelle concentration (c.m.c.) and the critical micelle temperature (c.m.t.) [2,3]. Usually, c.m.t. increases with increasing copolymer concentration, drawing a boundary line separating micelle region and unimer region in the temperature–concentration diagram, and the association number continuously increases with temperature and/or concentration going away from c.m.t. and/or c.m.c. However, it is not always the case. Some micellar solutions of block copolymers show unique phase behaviors different from such a simple behavior [4–12]. Micelle structure changes from spherical to elongated shape and, in some cases, giant particles or even precipitation have been observed in the transitional region near c.m.t., which is called anomalous micellization [6–11]. Zhou and Chu [8,9] have experimentally demonstrated that the anomalous micellization is a sort of phase separation induced by impurities of high molecular weight copolymers, while Sikora and Karasz [10] have tried to theoretically show that an immiscible region can exist in the transitional region to explain an origin of the anomalous micellization. The phase behavior of micellar solution near c.m.t. is complicate and needs further investigations to find general understandings of the behavior. Importance of understanding the behavior near c.m.t. can be pointed to have two aspects: one is to learn basic ordering processes of micelle formation from the unimer state, and the other is to elucidate a wide variety of micellization behaviors including "anomalous micellization", in weak association conditions. The micelle near c.m.t. is not frozen-in in a state far from the equilibrium state, and the history of its formation can clearly be defined. On the other hand, in strong association conditions, the micelle must have a non-equilibrium structure reflecting the structure in solid before dissolution into solvent [13–16], having a tightly-associated core which leads to a limit of micelle-size growth or change.

In this study, we investigate the micellization behavior of block copolymer solution near c.m.t. for polystyrene-*block*-poly(dimethylsiloxane) (PS-*b*-PDMS) in mixed solvent of 1,2-dichlorobenzene/benzyl alcohol. Light scattering experiments have revealed that the dilute solution with

* Corresponding author. Tel.: +81-3-5734-2132; fax: + 81-3-5734-2888.
E-mail address: tnose@polymer.titech.ac.jp (T. Nose).

0032-3861/00/$ - see front matter
PII: S0032-3861(99)00697-7

Table 1
Characteristics of the poly(styrene)-*block*-poly(dimethylsiloxane) sample

Sample	PS-block[a]	PDMS-block[b]	Total			
Code	M_w	M_n	M_n[b]	M_n[c]	M_w[d]	M_w/M_n[e]
SD-312	2900	11 800	14 700	12 500	15 000	1.23

[a] Size-exclusion chromatography (SEC) by PS-standard.
[b] Nuclear magnetic resonance for the copolymer with M_w of PS-block.
[c] SEC by PDMS-standard for the copolymer (correction made for composition-dependence of refractive index) with M_w of PS-block.
[d] Obtained from M_n(total) and M_w/M_n by SEC (PDMS-standard) for the copolymer (correction made for composition-dependence of refractive index).
[e] SEC by PDMS-standard for the copolymer (correction made for composition-dependence of refractive index).

concentration ranging from 0.08 to 4 wt% shows three different characteristic behaviors depending on the concentration. Furthermore, in the most concentrated region, a peak of the intensity has been found in the scattered light intensity–temperature diagram just below c.m.t., which is similar to the anomalous micellization. In the following sections, we will describe details of the experiments and the experimental data with their analyses. Then, discussion will be presented to suggest that the observed transitional change at the lower temperature region of the intensity peak may be explained by a strong condensation (collapse) of the core to form stable micelles due to the decrease in solvent quality with decreasing temperature.

2. Experiments

2.1. Materials

PS-*b*-PDMS was synthesized by sequential anionic polymerization. The trace of non-reacted PS homopolymer was removed using dimethylformamide. Characteristics of the PS-*b*-PDMS sample used are shown in Table 1.

The solvent was a mixture of 1,2-dichlorobenzene (DCB) and benzyl alcohol (BA). DCB and BA were of analytical grade and used without further purification. Both DCB and BA are selective solvents to PS, but BA is more strongly selective than DCB. One can adjust the c.m.t. by changing the composition of the mixed solvent. In this study, the composition was fixed at (DCB)/(BA) = 73.5/26.5 in weight, which set c.m.t. at about 100°C. In this mixed solvent the PDMS blocks may form a core to make an aggregate.

2.2. Light scattering measurements

The light scattering measurements were carried out with a home-built apparatus equipped with a He–Ne laser ($\lambda = 632.8$ nm) as light source and a photon detector (ALV/SO-SIPD). A sample tube was immersed in an index-matching oil bath thermoregulated to within ±0.05°C. The integrated scattered light intensity, I, from the solution was measured by photon counting at different scattering angles, θ, at 3° intervals in the range of 30°–120°.

The autocorrelation function of scattered light intensity was measured with an ALV-5000 multiple-τ digital correlator.

Optically clean solutions were prepared as follows. A solution of about 4 wt% of PS-*b*-PDMS was homogenized by stirring for 2 h at room temperature, and was filtered through 0.5 μm filters (Millipore) into a de-dusted light scattering cell. Then, an appropriate amount of the solvent was filtered through 0.1 μm filters directly into this cell to give desired concentration of solution by dilution, and the cell was flame-sealed under mild vacuum. Excess Rayleigh ratio $\Delta R(\theta)$ was calculated from the measured excess scattered-light intensity using the intensity of benzene as standard. The conventional analysis for determination of weight-average molecular weight and radius of gyration could not be applied to the present study because of associate-structure change with concentration and very large particle size, so that data analyses are performed on the basis of the following equation for the infinitely dilute solution [17].

$$\frac{KC}{\Delta R(\theta)} = \frac{1}{M_w P(\theta)} \tag{1}$$

M_w is the weight-average molecular weight, $P(\theta)$ the particle scattering function, C the polymer concentration in g/ml and K the optical constant defined by $K = 4\pi^2 n^2 (dn/dC)^2/(N\lambda^4)$, where n, λ and N are the refractive index of the solvent, the wavelength of incident beam and the Avogadro constant, respectively. The refractive index increment dn/dC was measured by a differential refractometer (Union Giken RM-102) to be expressed by $dn/dC = 0.1123 + 0.0001736(t/°C)$ in the unit of ml/g as a function of temperature t. Refractive indices are 1.55 and 1.55 for DCB and BA, respectively, being approximately isorefractive to each other, while those of PS and PDMS are 1.6 and 1.4, respectively. Because of small content of PS block and smaller difference of refractive index between PS and solvent, angular dependence of scattered-light intensity from the associates is approximately that of the PDMS part. Details of data analyses based on Eq. (1) will be described later.

The electric field correlation function $g^{(1)}(q,t)$ was calculated by the assumption of homodyne scattering. In cases of unimodal decay of $g^{(1)}(q,t)$, the second cumulant method was used to calculate the decay rate Γ and the variance μ_2/Γ^2. In cases of bimodal decay, the decay function of $g^{(1)}(q,t)$ was analyzed by the Laplace inversion program CONTIN [18] to separate the two modes and evaluate respective decay rates and amplitudes. The diffusion coefficient D was calculated by the relation $\Gamma = Dq^2$, where q is defined as $q = (4\pi n/\lambda)\sin(\theta/2)$. The extrapolation of D to zero

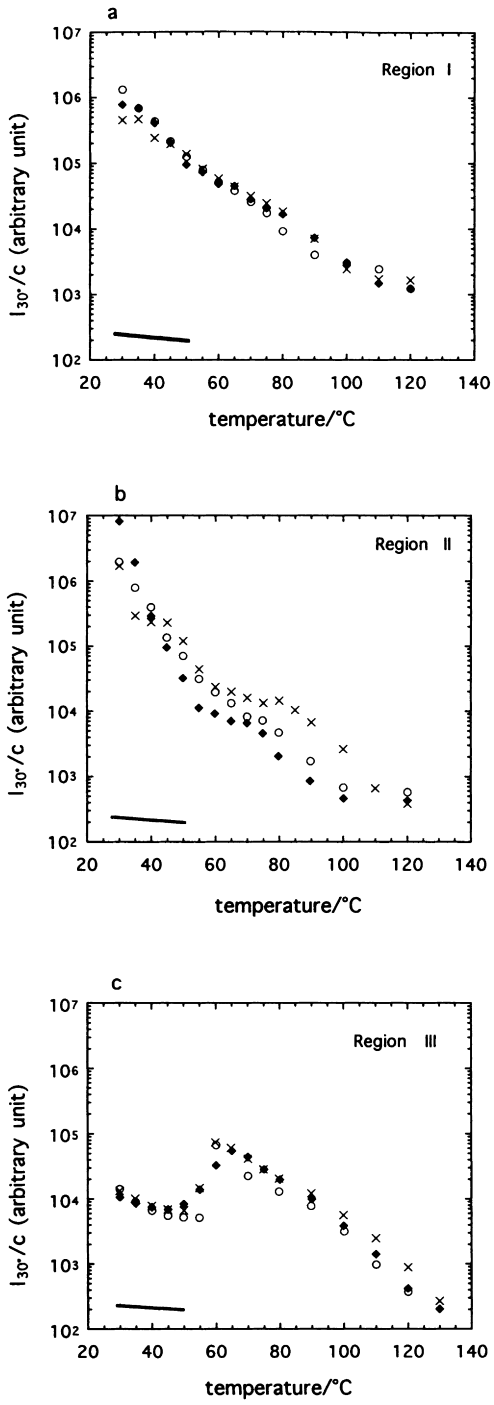

Fig. 1. Temperature dependence of scattered light intensity ($\theta = 30°$), $I_{30°}/c$, normalized by the concentration, c, for PS-*b*-PDMS solution in DCB/BA on heating in different concentration regions. Three distinct regions appear according to the copolymer concentration: (a) region I ($c =$ 0.0755 wt% (○), 0.107 wt% (×) and 0.216 wt% (◆)); (b) region II ($c =$ 0.442 wt% (○), 0.608 wt% (×) and 0.823 wt% (◆)); and (c) region III ($c = 1.04$ wt% (○), 2.27 wt% (×) and 4.16 wt% (◆)). Solid line indicates expected intensity of supposed unimer solution.

concentration was not applicable, so that apparent diffusion coefficient D at a finite concentration without the extrapolation was regarded as that at the dilute limit. From the apparent diffusion coefficient, apparent hydrodynamic radius R_h was calculated by the equation

$$R_h = \frac{k_B T}{6\pi\eta D} \tag{2}$$

where k_B, T and η are the Boltzmann constant, absolute temperature and solvent viscosity, respectively. The solvent viscosity was measured by an Ubbelohde-type viscometer as a function of temperature.

The light scattering experiments were carried out by the following procedures of temperature history unless specially mentioned. Before starting the experiments, the solution was kept at 130°C for 2 h to be homogenized free from any aggregation. In the heating experiments, the solution was quenched from 130 to 30°C, then the light scattering measurements were made at every 5°C up to 80°C, and at every 10°C from 80 to 130°C, taking 1 h for one experimental run to the next higher-temperature run. In the cooling experiments, the measurements were carried out at every 10°C from 130 to 80°C and then at every 5°C down to 30°C, taking 1 h for each run.

3. Results and discussion

Fig. 1 shows the temperature dependence of the scattered light intensity, I, divided by the concentration, c, upon heating as a function of c. Here is also indicated the intensity expected if the solution were free from any aggregation, which was calculated from the molecular weight of unimers with approximations of the dilute limit ($C \to 0$), and the small particle size limit ($P(30°) = 1$ because of $R_g q \ll 1$ for unimers). We can see three concentration regions exhibiting different behaviors. In Region I of dilute solutions ($0.07\text{wt\%} < c < 0.2\text{wt\%}$), the intensity monotonically decreases with increasing temperature, showing almost no concentration dependence of the reduced intensity I/c, while in Region II of intermediate concentrations ($0.4\text{wt\%} < c < 0.8\text{wt\%}$) the intensity decreases showing a shoulder around 80°C, with I/c decreasing with increasing concentration. The interesting region is Region III of high concentrations ($1.0\text{wt\%} < c < 4.2\text{wt\%}$), where the intensity shows a transitional change making a peak right below the unimer region, having almost no concentration dependence on I/c. This is similar to anomalous micellization. Detailed behavior in respective regions will be described below.

3.1. Region I ($0.07\text{wt\%} < c < 0.2\text{wt\%}$)

Fig. 2 indicates that the temperature dependence of intensity on cooling somewhat differs from that observed upon heating, so that the intensity change is not exactly reversible. One can more directly see the irreversibility in the time-dependence of intensity at 30°C after quench from 120°C, as shown in Fig. 3. The intensity grows quickly, then decreases very slowly exhibiting a peak, and tends to level off approaching the equilibrium value. This may

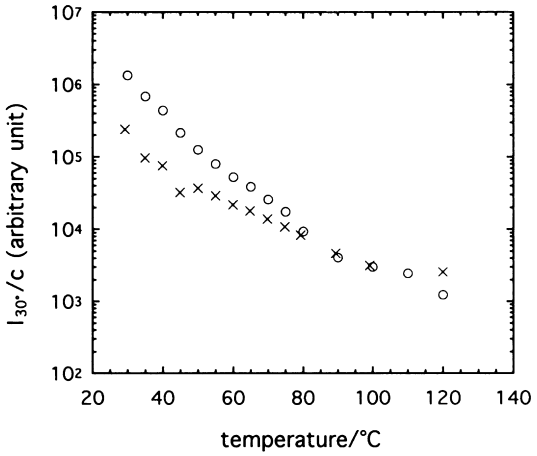

Fig. 2. Temperature dependence of scattered light intensity ($\theta = 30°$), $I_{30°}/c$, for PS-*b*-PDMS solution of $c = 0.0755$ wt% in Region I on heating (○) and cooling (×).

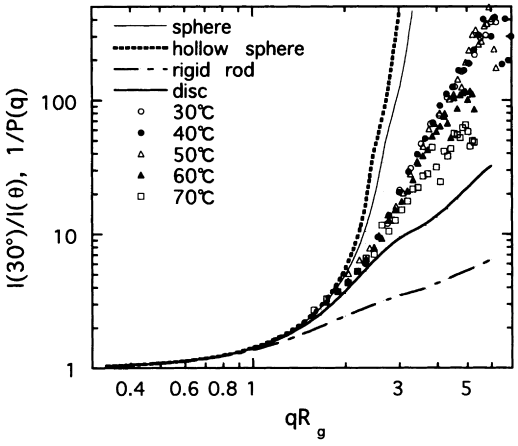

Fig. 4. Inverse of scattered-light intensity $I(30°)/I(\theta)$ plotted against $R_g q$ for $c = 0.0755$ wt% at various temperatures compared with inverse of particle scattering function $1/P(q)$ vs. qR_g relations for some simple models.

indicate that the equilibrium intensity is lower than those observed on heating or cooling, which leads to the process dependence shown in Fig. 2. That is, the intensity for heating of the quenched solution is higher than that for the solution under slow cooling. At any rate, the micelles observed on heating or cooling are not really equilibrium ones, but those formed in the course of micellization.

In Fig. 4, the q-dependence $I(q)$ of the intensity is compared with particle scattering functions $P(q)$ of some typical particle shapes by log–log plots of inverse $I(q)$ and inverse $P(q)$ against $R_g q$ with R_g being the radius of gyration. Here, the values of R_g were appropriately chosen so as to give likely q-dependencies. It should be noted that the values of $1/I(q)$ are plotted in arbitrary units and the fraction and the molecular weight of aggregates, which determine the absolute value of $I(q)$, are unknown. Therefore, the plots were shifted vertically by an appropriate distance to fit $1/P(q)$ curves. The experimental results for q-dependence of $I(q)$ seem closest to the spherical (or hollow spherical) $P(q)$.

The correlation function $g^{(1)}(t)$ of dynamic light scattering shows single mode decay. The decay rate approximately follows q^2-dependence. Obtained hydrodynamic radii R_h are presented as a function of temperature in Fig. 5, along with the R_g used in Fig. 4 and the ratio of R_g/R_h. The particle size is a few 100 nm, and it decreases gradually as the temperature increases. The estimated ratio of R_g/R_h is close to unity, suggesting the shape of particles to be (hollow) spherical, which is consistent with the results of static experiments. Therefore, the particles are most likely spherical.

3.2. Region II (0.4wt% < c < 0.8wt%)

In this region, where the intensity has complex temperature

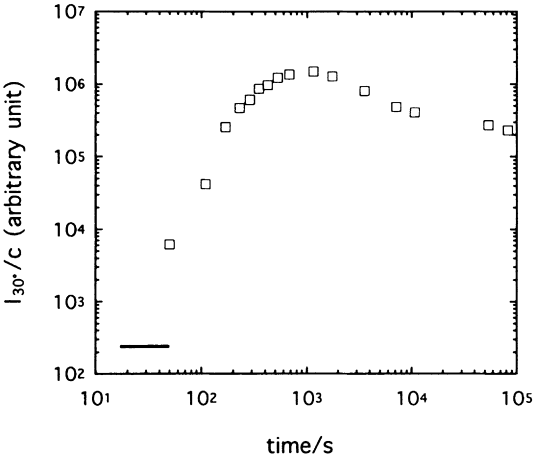

Fig. 3. Time evolution of scattered light intensity ($\theta = 30°$), $I_{30°}/c$, for $c = 0.0755$ wt% at 30°C after quenching from 120°C. Solid bar indicates expected intensity of supposed unimer solution.

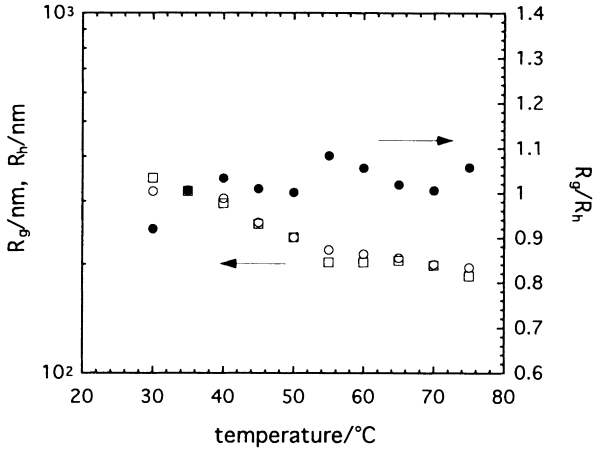

Fig. 5. Temperature dependencies of R_g (estimated under the assumption of spherical particles), R_h and their ratio R_g/R_h for $c = 0.0755$ wt%. R_g (○), R_h (□) and R_g/R_h (●).

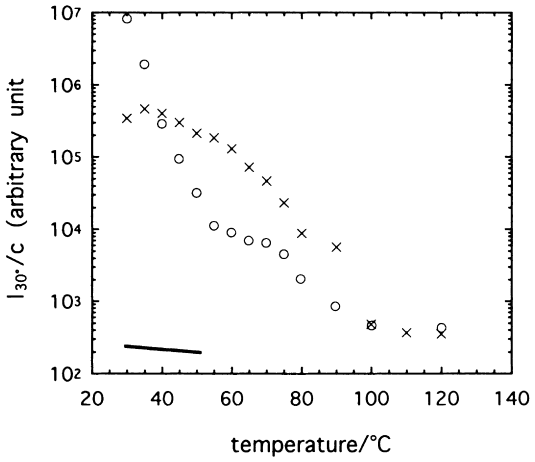

Fig. 6. Temperature dependence of scattered light intensity ($\theta = 30°$), $I_{30°}/c$, for PS-*b*-PDMS solution of $c = 0.0823$ wt% in Region II on heating (○) and cooling (×). Solid line indicates expected intensity of supposed unimer solution.

and concentration dependencies, it also exhibits a complicate heating–cooling process dependence, as shown in Fig. 6. The intensity for heating is lower than that for cooling, in contrast to the behavior in Region I. Time evolution of the intensity and R_h for the quenched solution at 30°C are presented in Fig. 7. The intensity quickly increases followed by level off for a while, and then decreases down to those, which are lower than that expected for the unimer solution. On the other hand, at the later stage the hydrodynamic radius decreases much more gradually than the intensity does. These results of Fig. 7 suggest precipitation of large particles at the later stage. Precipitation may explain the process-dependence presented in Fig. 6. Namely, the solution quenched to 20°C shows very high intensity because of formation of large particles, and the decrease of intensity with start of increasing temperature is accelerated by precipitation, resulting in the lower intensities around 60°C. On the contrary, upon cooling, the intensity increases by growth of the associates with cooling, and at low temperatures the particle size becomes so large that precipitation takes place, which results in lowering of the intensity at temperatures lower than about 40°C. The higher the concentration, the easier the precipitation may occur. This may lead to the concentration-dependence shown in Fig. 1(b).

Temperature dependencies of R_h and μ_2/Γ^2 on heating for the highest concentration in Region II are shown in Fig. 8. At lower temperatures, the hydrodynamic radius is very large, the largest reaching a few 1000 nm. However, the particle-size distribution is very broad, giving the second cumulant moment of μ_2/Γ^2 as being more than unity. At temperatures higher than 60°C, the hydrodynamic radius has a much narrower distribution and is a few 100 nm comparative to the size in Region I. This may imply the precipitation of larger particles during the heating process.

3.3. Region III (1.0wt% < c < 4.2wt%)

As shown in Fig. 9, the intensity change with temperature is almost reversible, although the slight difference observed above 60°C is similar to those found in Region II. The temperature T_t at the discontinuous change is about 60°C independent of concentration and heating/cooling processes.

Decay rate distributions of the dynamic correlation function $g^{(1)}(t)$ are shown in Fig. 10. The results clearly show the presence of two modes; the intensity amplitude of the large decay rate (fast mode) decreases with increasing temperature, while that of the small decay rate (slow mode) increases and the decay becomes substantially unimodal at 70°C. The q-dependencies of decay rates for both slow and fast modes obey the q^2-dependence of simple diffusion. The bimodal behavior is also seen in $I(q)$ of static light scattering, which are shown as a function of temperature in Fig. 11.

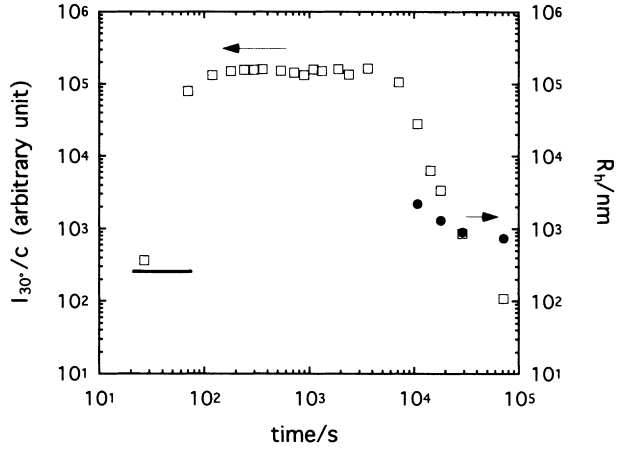

Fig. 7. Time evolution of scattered light intensity ($\theta = 30°$), $I_{30°}/c$, and hydrodynamic radius R_h for $c = 0.0823$ wt% at 30°C after quenching from 120°C: $I_{30°}/c$ (□) and R_h (●). Solid bar indicates expected intensity of supposed unimer solution.

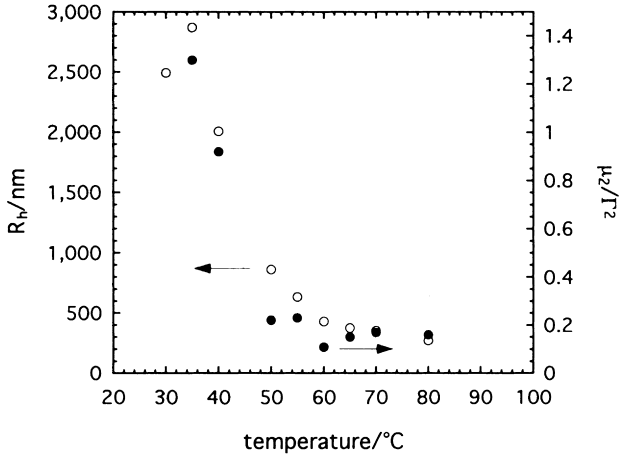

Fig. 8. Temperature dependencies of R_h (○) and μ_2/Γ^2 (●) for $c =$ 0.0823 wt% in Region II on heating.

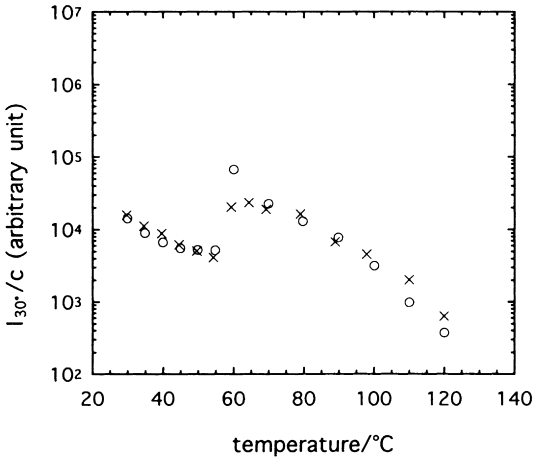

Fig. 9. Temperature dependence of scattered light intensity ($\theta = 30°$), $I_{30°}/c$, for PS-*b*-PDMS solution of $c = 1.04$ wt% in Region III on heating (○) and cooling (×).

The intensity profiles $I(q)$ seem to consist of a weak intensity of a weak q-dependence and a strong intensity at low q-values. Assuming a bimodal distribution and solid spherical particles, experimental $I(q)$ is fit to the following equation based on Eq. (1) [17].

$$\frac{KC}{\Delta R(\theta)} = (A^{\text{large}}(\theta) + A^{\text{small}}(\theta))^{-1} \tag{3}$$

where

$$A^{\text{large}}(\theta) = A^{\text{large}}(0)\left[\frac{3}{X_l^2}(\sin X_l - X_l \cos X_l)\right]^2$$

$$A^{\text{small}}(\theta) = A^{\text{small}}(0)\left[\frac{3}{X_s^2}(\sin X_s - X_s \cos X_s)\right]^2 \tag{4}$$

with

$$X_l = R_{\text{large}}q; \qquad X_s = R_{\text{small}}q \tag{5}$$

It should be noted here that Eq. (3) based on Eq. (1) holds for the infinitely dilute limit, neglecting the effects of the inter-particle interference of scattered light. Therefore, quantitative reality of the fitting results may be poor because the solutions are rather concentrated. An example of the fitting by least-squares fitting is shown in Fig. 12. The bimodal analysis works well to yield the radii, R_{large} and R_{small}, and the intensity fraction $\alpha(\theta)$ of large particles, $\alpha(\theta) = A^{\text{large}}/(A^{\text{large}} + A^{\text{small}})$. Fractions α and the radii of large and small particles are shown as functions of temperature in Figs. 13 and 14, respectively. The results obtained from both static- and dynamic-scattering are reasonably consistent with each other, which rationalizes the present data analyses. The fractional contribution from large particles increases with increasing temperature, reaching almost unity around 60°C. Considering that the intensity at a low angle from large particles is much higher than that from small particles at a fixed mass concentration

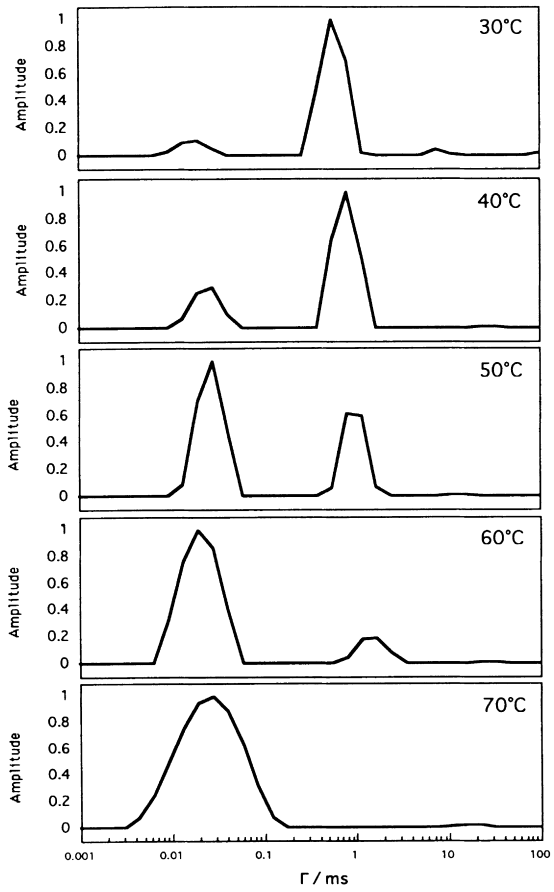

Fig. 10. Decay-rate distributions of dynamic light scattering for PS-*b*-PDMS solution of $c = 4.16$ wt% at different temperatures.

because of large particle mass, the amount of large particles is very subtle below $T_t \cong 60$°C) and then sharply increases around T_t. Therefore, the appearance of large particles exactly corresponds to the occurrence of the transitional change of intensity. It is noteworthy to point out that two

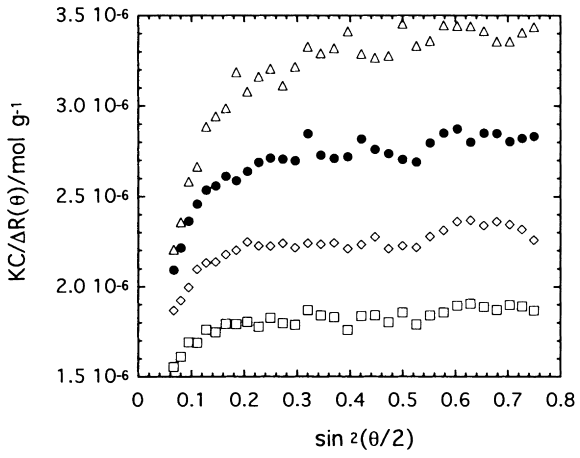

Fig. 11. Zimm-type plots of angular dependence of scattered light intensity, $KC/\Delta R(\theta)$ vs. $\sin^2(\theta/2)$, for $c = 4.16$ wt% at lower temperatures: 30°C (□), 35°C (◇), 40°C (●) and 45°C (△).

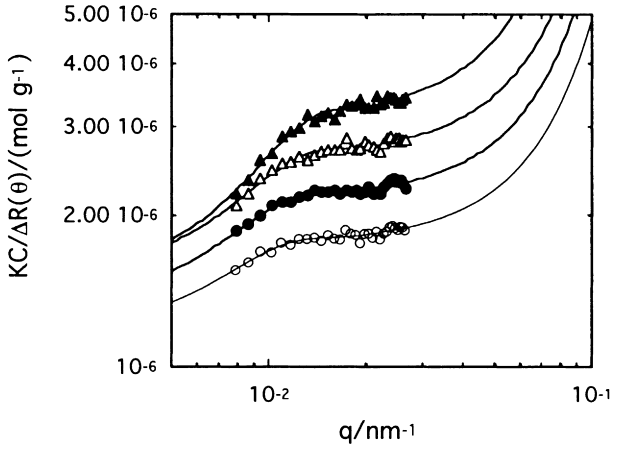

Fig. 12. Bimodal fittings of angular dependence of scattered light intensity, $KC/\Delta R(\theta)$ vs. q for $c = 4.16$ wt% at lower temperatures: 30°C (○), 35°C (●), 40°C (△) and 45°C (▲). Solid lines are the fitting curves to Eq. (3).

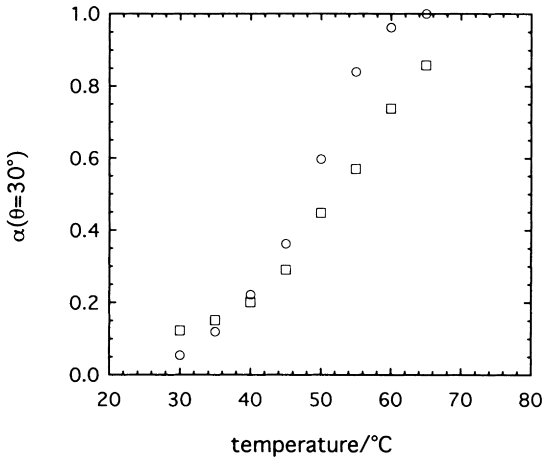

Fig. 13. Temperature-dependence of fractional amplitude $\alpha(\theta = 30°)$ of the slow-mode due to large particles for $c = 4.16$ wt% : static light scattering (□) and dynamic light scattering (○).

types of associates with largely different sizes coexist. In this sense, the change is really transitional, i.e. discontinuous. The radii of large particles are about 400 nm[1], while those of the small particles formed at low temperatures of $T < T_t$ are about 10 nm. These sizes are independent of temperature. Considering the large particle size compared with the copolymer molecular size, the large particles may have a hollow spherical shape. It should be noted here that unfortunately we do not know the real amount of large particles appearing above $T \geq T_t$ since we can only know the intensity contribution from light scattering. On the contrary, the scattered light intensity is still increasing in the lower temperature range of $T < T_t$ as the temperature decreases, while the particle size is stationary. This may suggest that the particles become more compact with decreasing temperature because of increasing association strength of core blocks.

In conclusion, in Region III the particle radius is small, about 10nm at the lower temperature range of $T < T_t (\approx 60°C)$. At about 60°C, the radius becomes large very quickly up to of the order of 100 nm. The coexistence of large and small particles is detected by static and dynamic light scattering as bimodal behavior.

4. General discussion

The transitional change in particle size in Region III yields a high-intensity peak in light scattering near c.m.t., which is similar to anomalous micellization. This association behavior may be rather common in many types of block copolymer micellar solutions near c.m.t. Near c.m.t., the selective solvent quality is not so bad for core blocks to form a tightly bonded core, but the core may be swollen with solvent, or can even be a hollow spherical core. This situation can make it possible to form large-size particles such as swollen, hollow micelles or vesicle near c.m.t. In this context, the phenomenon observed here can be explained as follows.

As the temperature decreases from the unimer state into the micellar region, very large particles are formed first. Then, as the core association becomes stronger due to solvent quality getting worth with further decrease in temperature, less swollen and/or smaller hollow core becomes more stable, which leads the transitional change from large hollow spherical micelles to small compact micelles. With further decrease of temperature, the swollen core becomes less swollen and more compact probably accompanied with increasing association number. This explanation may be applicable to some other cases of anomalous micellization.

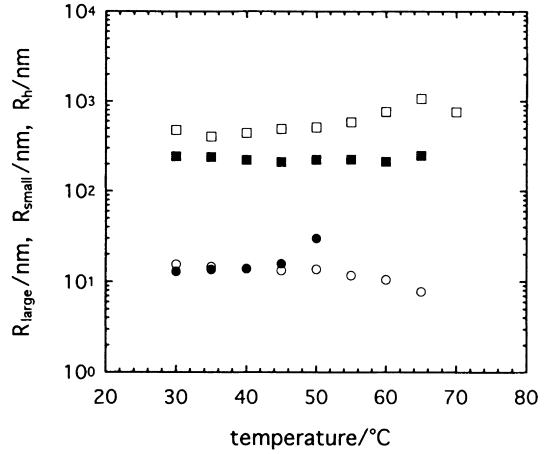

Fig. 14. Temperature-dependencies of R_g, and R_h for $c = 4.16$ wt% : R_g (●, ■), R_h (○, □), small particles (●, ○) and large particles (■, □). (See a note in the text about the values of R_h for large particles.)

[1] The particle size evaluated by dynamic-scattering here is the size for the particles radiating the light of the maximum-scattered intensity for respective modes, so that the real representative size averaged by weight, for example, should be smaller than this value, say about half or less, for the large particles with this much width of size distribution.

A question arising here is whether the transition is a two-state transition from one thermodynamically stable micelle to another. The discrete bimodal distribution of micelle size seems to suggest the two-state transition, although the transition occurs reversibly at the same temperature in heating and cooling, i.e. no appreciable super-cooling is observed.

Large micelles formed at lower concentrations and lower temperatures are not equilibrium ones as suggested before, so they may kinetically appear by rapid quench to lower temperatures. It has been reported that very large micelles can be formed in kinetic processes at low concentrations [12].

Theoretical approaches are now in progress; we are theoretically studying a possibility of the change between expanded and shrunken micelles from a micelle stability aspect and investigating large micelle formation from a kinetic aspect. Obtained results of the theoretical study from stability supports the above explanation, which will be reported elsewhere [19].

5. Conclusions

We have investigated micelle-forming behavior in diblock copolymer solutions near the critical micelle temperature, by means of static and dynamic light scattering, to see how the copolymers start to form micelles and become strongly associated ones as the aggregation ability increases. As results, we have demonstrated the following. We have observed three concentration regions.

1. In dilute solutions at relatively high concentrations of Region III, the diblock copolymer forms a large spherical hollow micelle, which exhibits a transitional change in size from expanded to compact associates with decreasing temperature. This may be a possible explanation of the anomalous micellization.
2. In the transition region, the particle-size distribution is bimodal, indicating the coexistence of compact and expanded micelles.
3. With decreasing temperature, the compact micelle shows the increase of scattered-light intensity (accordingly maybe increases its association number), keeping the size almost constant, which may indicate that the micelle becomes more compact.
4. At lower concentrations of Regions I and II, the micelle does not show the collapse, with the size increasing with decreasing temperature.
5. The large micelles observed at lower temperatures in Regions I and II are not equilibrium ones, but appear kinetically. During faster cooling, the larger micelles are temporally formed.
6. If the large micelles become large enough, they precipitate eventually. The precipitation is clearly seen at intermediate concentrations at lower temperatures.

References

[1] Tuzar Z, Kratochvíl P. In: Matijevi E, editor. Surface and colloid science, 15. New York: Plenum Press, 1993. p. 1–83.
[2] Elias HGJ. In: Huglin MB, editor. Light scattering from polymer solutions, New York: Academic Press, 1972.
[3] Leibler L, Orland H, Wheeler JC. J Chem Phys 1983;79:3550.
[4] Tsunashima Y. Macromolecules 1990;23:2963.
[5] Yu Y, Zhang L, Eisenberg A. Macromolecules 1998;31:1144.
[6] Tuzar Z, Stepanek P, Koák C, Kratochvil P. J Colloid Interface Sci 1985;105:372.
[7] Yeung AS, Frank CW. Polymer 1990;31:2089.
[8] Zhou Z, Chu B. Macromolecules 1987;20:3089.
[9] Zhou Z, Chu B. Macromolecules 1988;21:2548.
[10] Sikora A, Karasz FE. Macromolecules 1993;26:177.
[11] Iyama K, Nose T. Polymer 1998;39:651.
[12] Iyama K, Nose T. Macromolecules 1998;39:7356.
[13] Price C, Chan EKM, Hudd AL, Stubbersfield RB. Polym Commun 1986;27:196.
[14] Stejskal J, Hlavatá D, Sikora A, Koák C, Pletil J, Kratochvíl P. Polymer 1992;33:3675.
[15] Stejskal J, Koák C, Helmstedt M, Kratochvíl P. Collect Czech Chem Commun 1993;58:2282.
[16] Hlavatá D, Stejskal J, Pletil J, Koák C, Kratochvíl P, Helmstedt M, Mio H, Laggner P. Polymer 1996;37:799.
[17] Burchard W. In: Burchard W, Patterson GD, editors. Light scattering from polymers, Berlin: Springer, 1983.
[18] Provencher SW. Comput Phys Commun 1982;27:213–29.
[19] Nose T, Numasawa N. In preparation.